FEBS *Letters*

Multiparametric image analysis reveals role of Caveolin1 in endosomal progression rather than internalization of EGFR

Hannah Schmidt-Glenewinkel [a,*], Eileen Reinz [b], Svetlana Bulashevska [a], Joel Beaudouin [a], Stefan Legewie [a,d], Angel Alonso [b], Roland Eils [a,c,*]

[a] Theoretical Bioinformatics, German Cancer Research Center, 69120 Heidelberg, Germany
[b] Tumor Virology, German Cancer Research Center, 69120 Heidelberg, Germany
[c] Institute for Pharmacy and Molecular Biotechnology, University of Heidelberg, 69120 Heidelberg, Germany
[d] Institute of Molecular Biology, Mainz, Germany

ARTICLE INFO

ABSTRACT

Endosomes constitute a central layer in the regulation of growth factor signaling. We applied flow cytometry, confocal microscopy and automated image quantification to define the role of Caveolin1 (Cav1) in epidermal growth factor (EGF) receptor (i) internalization and (ii) endosomal trafficking. Antisense-downregulation of Cav1 did not affect internalization of EGF:EGFR-complexes from the plasma membrane. Instead, Cav1-knockdown had a profound effect on endosomal trafficking and caused a shift in EGF vesicle distribution towards Rab7-negative compartments at late timepoints. Moreover, image quantification with single-endosome resolution revealed that EGF:Cav1-complexes undergo a maturation pattern reminiscent of late endosomes. Our data suggest a model in which Caveolin1 acts upon EGF endosomes internalized via the Clathrin-pathway and functions at the transition from early to late endosomes.

© 2012 Published by Elsevier B.V. on behalf of the Federation of European Biochemical Societies.

1. Introduction

Endocytosis constitutes an important regulatory layer for receptor tyrosine kinases (RTKs) (reviewed in [1,2]). The EGF receptor (EGFR), a member of the ErbB family of receptors, is one of the best-characterized RTKs [3]. In response to ligands, ErbB receptor tyrosine kinases induce a variety of cellular responses, including proliferation, differentiation and motility [4]. EGF-binding induces receptor homodimeriztaion and activation of tyrosine kinase activity, which results in the initiation of intracellular signal transduction pathways [5,4]. Within minutes after activation, ligand–receptor complexes undergo endocytosis [6,7]. Endocytosis can be subdivided into two steps: the initial step is internalization, that is, translocation of cargo from the cell surface into intracellular vesicles. Internalization mainly controls the number of cell surface receptors and thus the sensitivity of the cell to incoming signal. In the subsequent phase of endocytic trafficking, internalized receptors are sorted through a complex system of intracellular vesicle compartments, known as endosomes (reviewed in [1,5,8]). From early endosomes, which are characterized morphologically by

small size and proximity to the plasma membrane [9], incoming ligand–receptor complexes are sorted to different recycling or degradation compartments. Endosomes carry active receptors [6,10], implying that the exact location and timely progression through endocytic compartments is critical for controlling signal specificity and duration [6,11,12]. Dysfunctional regulation of EGFR endocytosis can promote uncontrolled growth, most likely by enhancing steady state EGFR signaling and proliferation [2]. Thus, the dissection of the endosomal network is a primary need in order to understand signaling control. Since biochemical methods fail to separately analyze the different types of vesicles, quantitative imaging is needed to properly analyze the intracellular steps followed by internalized receptors.

Several internalization pathways have been postulated for EGFR [13,14]. Clathrin-mediated internalization, also known as the coated pit pathway [15–17], is the major mechanism for the initial internalization step. A number of essential adaptor proteins such as AP180 [18] recruit receptors to clathrin-coated vesicles [17,19], which pinch off by action of the GTPase dynamin [20].

A second putative internalization pathway relying on Caveolae has been described [21]. Caveolae-mediated endocytosis describes a clathrin-independent internalization pathway, in which Caveolin-1 (Cav1) containing vesicles traffic between the plasma membrane and intracellular pools [22,23]. Two Caveolae-trafficking

* Corresponding authors. Current address: Department of Molecular Genetics, Weizmann Institute of Science, Rehovot, Israel (H. Schmidt-Glenewinkel).
E-mail address: hannahsg@weizmann.ac.il (H. Schmidt-Glenewinkel).

routes have been described so far: in a short loop, Cav1-vesicles cycle between the plasma membrane and cytosol, but remain restricted to a small volume underneath the cell surface. In a second mode, certain cues can trigger the long-range cellular transport, in which Cav1-vesicles can associate with early endosomes in a process regulated by small GTPases [24,25].

The following lines of evidence argue for a role of Caveolae-endocytosis as an independent internalization pathway for EGFR: (i) residual EGFR internalization occurs upon inhibition of clathrin-dependent endocytosis [13,14,26,27], (ii) co-localization between endosomal EGFR and Cav1 has been observed [13,28], (iii) treatment of cells with filipin, a cholesterol-depleting drug disrupting Caveolae, reduces EGFR internalization [14]. Nevertheless, conflicting results have been published reporting that downregulation of clathrin heavy chain efficiently prevents EGFR internalization [26,29,30]. It is, however, difficult to conclude whether incomplete block of internalization stems from incomplete clathrin knockdown or from the existence of alternative pathways.

An intriguing alternative for the role of Cav1 in EGFR endocytosis is suggested by observations about the trafficking behaviour of certain viral ligands. Cholera Toxin virus and JC virus enter cells via Clathrin-mediated internalization and are sorted intracellularly from early endosomes to the caveolar trafficking pathway [31,32].

Thus, it is of great interest to understand the role of Cav1 in the regulation of growth factor receptor processing. A large body of evidence implies Cavl in the downregulation of growth factor signaling and suggests that it acts as a tumor suppressor [33,34]. Antisense downregulation of Cav1 is sufficient to induce cell transformation [35]. Conversely, ectopic expression of wild type Cav1 in oncogene transformed cell lines suppresses anchorage-independent growth and invasiveness [36,37]. Further, downstream signaling of the EGFR is negatively regulated by Cav1 in pancreatic cancer cells [38]. These observations strongly suggest that Cav1 plays a role in the attenuation of growth factor signaling.

To this date, the role of Caveolae-endocytosis has not beend studied level in the context of endosomal trafficking of the EGFR rather than related to EGFR internalization. Here, we developed a quantitative single-endosome imaging framework and applied it to analyze the role of Caveolin-1 in EGF endosomal trafficking. We show that Cav1 plays a role in late endosomal progression of internalized EGF.

2. Results

2.1. Cav1 is not required for efficient internalization of the EGFR

A clathrin-independent internalization mechanism via caveolin-enriched plasma membrane domains has been proposed for EGFR [13,14,28]. In order to determine the role of Caveolin1 (Cav1) in EGFR internalization, we downregulated Cav1 using shRNA [32] and determined surface-EGFR using flow cytometry. In order to estimate the single-cell efficiency of the knockdown, we performed immunoflourescence against Cav1 in control- or shCav1-transfected cells and quantified the staining intensity from whole-cell confocal microscopy image stacks (Fig. S1A–C). The estimated efficiency of the shRNA-mediated knockdown of Cav1 was 75% (Fig. S1D). In order to be able to select transfected cells in the flow cytometric measurement, we co-transfected cells with a BFP-marker and the control or Cav1 shRNA plasmid. The reliability of BFP to serve as a marker for shCav1 expression was tested for in a co-transfection assay in HeLa cells stably expressing GFP-Cav1 and verified by flow cytometry (Fig. S1E).

Analysis of the EGF-induced downregulation of surface-EGFR in Cav1 knockdown cells (Fig. 1A, blue) revealed no difference to the cells expressing a control vector (Fig. 1A, black). We also performed

the complementary experiment and monitored uptake of Rhodamine-labeled EGF using flow cytometry (Fig. 1B). For this, we followed the acid-wash protocol previously described [7], which allows to discriminate between surface-bound and internalized EGF. Again, Cav1 knockdown cells (Fig. 1B, blue) showed the same amount of internalized EGF up to 30 min as control cells (Fig. 1B, black). This data shows that reduction of Caveolin1 levels does
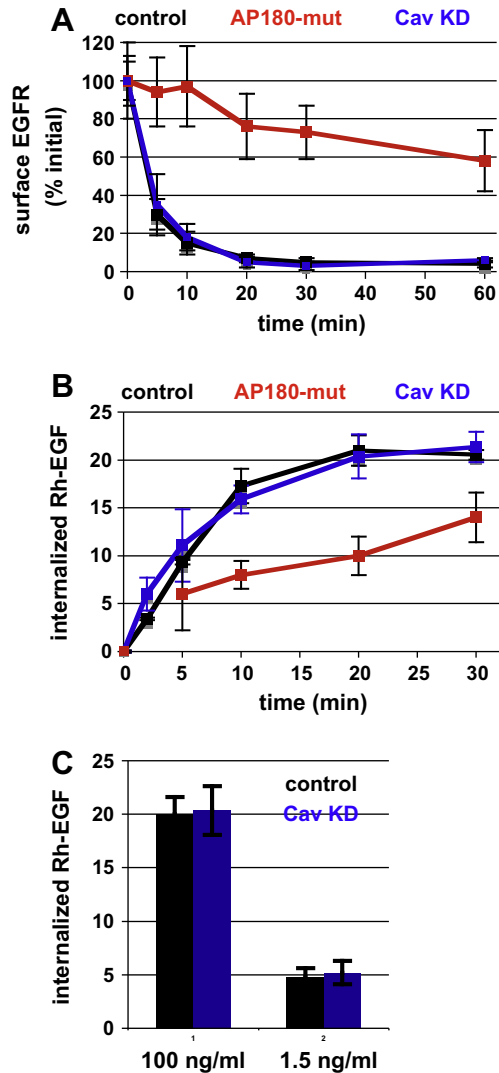
Fig. 1. Cavl is not required for efficient internalization of the EGFR. (A) Inhibition of Clathrin-mediated endocytosis, but not Caveolin1 depletion decreases EGFR internalization. Flow cytometric detection of surface EGFR. HeLa cells were co-transfected with BFP and shCav1-plasmid in a 1:2 ratio (blue), a control vector (gray) and AP180mut-IRES-GFP vector (red), respectively. Cells were stimulated with 100 ng/ml EGF continuously for indicated time points and surface EGFR was determined by antibody staining followed by flow cytometry (see Section 4). Per measurement, 10,000 cells were evaluated. To select Cav1-KD cells, BFP-positive cells were gated for. To select AP180mut-expressing cells, GFP-positive cells were gated for. Shown is mean value of two measurements, error bars denote standard deviation. (B) Inhibition of Clathrin-mediated endocytosis, but not Caveolin1 depletion decreases uptake of Rhodamine-EGF Flow cytometric detection of Rhodamine-EGF. HeLa cells were transfected as in A. Cells were stimulated with 100 ng/ml Rhodamine-EGF continuously for indicated time points, washed with acid buffer and uptake of Rhodamine-EGF was determined by flow cytometry (see Section 4). Per measurement, 10,000 cells were evaluated. Shown is mean value of two measurements, error bars denote standard deviation. (C) Flow cytometric detection of Rhodamine-EGF after 20 min. HeLa cells were transfected as in A. Cells were stimulated with 100 ng/ml or 1.5 ng/ml Rhodamine-EGF for 20 min and subjected to flow cytometry. Shown is mean value of two measurements, error bars denote standard deviation.

not affect the initial internalization step in EGFR endocytosis. We found this result to be independent of the EGF concentration used. In Fig. 1C we plot the amount of internalized Rhodamine-EGF after 20 min of stimulation with 100 ng/ml or 1.5 ng/ml. While, expectedly, the total amount of internalized Rhodamine-EGF is lower when stimulated with low amounts, no difference is seen between control or Cav KD cells (Fig. 1C, right).

AP180 is an essential adaptor of the clathrin-mediated internalization pathway [18]. In order to verify the sensitivity of our internalization assay we expressed a dominant-negative mutant of AP180 (AP180mut). We found that: (i) internalization of surface EGFR was strongly delayed in AP180mut-expressing cells (Fig. 1A, red) and (ii) the strength of this delay was more pronounced in cells expressing higher levels of AP180 (not shown). The latter conclusion could be drawn from the fact that our expression vector contains an AP180mut-IRES-GFP-sequence so that GFP-expression scales with expression of the AP180-mutant. Similarly, we found that uptake of Rhodamine-EGF was strongly impaired in AP180mut-expressing cells using flow cytometry (Fig. 1B, red). This data confirms the sensitivity of our internalization assay.

Together, this shows that inhibition of Clathrin-mediated internalization, but not downregulation of Cav1 lowers the rate of EGF-induced EGFR-internalization.

2.2. Specific colocalization between EGF endosomes and Cav1-vesicles increases during endocytic trafficking

Even though Cav1 is not required for EGF-induced internalization of EGFR, it might still be involved in endosomal trafficking of internalized EGF:EGFR complexes. To investigate this, we evaluated co-localization between Rhodamine-labeled EGF and Cav1 in HeLa cells stably expressing GFP-Cav1 (GFP-Cav1 cells) (see Fig. 2). Fig. 2A shows GFP-Cav1 expressing cells, which were fixed after different durations of stimulation with Rhodamine-EGF. It can be seen that after 2 or 5 min of stimulation, no or little co-localization between EGF- and Cav1-vesicles is observed. In contrast, after 10 and 20 min, a much more pronounced co-localization between EGF- and Cav1- vesicles (indicated in yellow) is seen.

To gain more quantitative insight into the temporal evolution of co-localization, we applied automated image analysis. For this, we detected vesicles from segmented microscopy images in an automated manner (see Section 4). A central problem in co-localization studies is specificity. To address this, we performed three control experiments. As a positive control, we stimulated HeLa cells transfected with GFP-EGFR by Rhodamine-EGF and determined colocalization between detected vesicles from both color channels (see Section 4 for details of co-localization analysis). We found that up to 20 min, about 85% of EGF vesicles colocalized with a GFP-EGFR vesicle (Fig. 2B, dark gray; Fig. S2A), confirming that our measure captures true co-localization events. As a negative control for co-localization, we stimulated GFP-Cav1 expressing cells with Alexa546-Transferrin and determined colocalization between vesicles at different timepoints for up to 20 min (Fig. 2B, light gray). Transferrin is known to internalize exclusively via the clathrin-dependent pathway [39]. In a time-invariant manner less than 10% of transferrin-vesicles showed co-localization with Cav1 vesicles (Fig. 2B, light gray; Fig. S2B). We conclude that our method of co-localization detection is able to discriminate between specific and unspecific colocalization. As a final control, we analyzed the temporal evolution of co-localization between Rhodamine-EGF and GFP-clathrin in HeLa cells stably expressing GFP-clathrin heavy chain (HC) [40]. The clathrin protein forms cage-like structures, which disassemble immediately after internalization [41]. As expected, colocalization between EGF and Clathrin-HC was transient and occurred in the early (<=10 min) phase of internalization (Fig. 2C, Fig. S3A and S3B). This is consistent with EGF-induced

EGFR-internalization being complete after 10–15 min in HeLa cells [7]. Having established the reliability of our co-localization assay, we analyzed the fate of vesicles containing Cav1 and/or EGF. In contrast to Clathrin, Caveolin1 colocalization with EGF occurs late in endocytosis. Whereas after 2 min of stimulation only about 15% of EGF vesicles co-localize with Caveolin1, this fraction increases progressively to about 58% after 20 min of stimulation (Fig. 2C, black).

It was proposed in previous studies that Caveolae-mediated endocytosis of EGF occurs specifically when cells are stimulated with high concentrations of EGF [13,42]. To test this, we stimulated GFP-Cav1 expressing cells with increasing amounts of EGF from 1 to 100 ng/ml and evaluated co-localization after 20 min of stimulation. We found that, while the overall number of EGF endosomes increases with increasing stimulation, the fraction of co-localization with Cav1 is independent of EGF-concentration (Fig. S4). Taken together, the presented data show that colocalization between EGF- and Caveolin1-vesicles is specific and increases as endocytic trafficking progresses.

2.3. EGF/Cav1-colocalization shows a spatial gradient towards the perinuclear region

Previous work indicated that the Caveolae-pathway can act as long-range transport device for internalized ligands [43,44]. In this trafficking mode, Cav1-vesicles are internalized from the plasma membrane pool to intracellular organelles and traffic away from the periphery towards the perinuclear region [24]. In contrast, Caveolin1 trafficking in unstimulated cells is restricted to a small volume underneath the cell surface [22,43]. We therefore hypothesized that Cav1 vesicles co-localizing with EGF are shifted to the perinuclear region when compared to Cav1 vesicles not associated with EGF.

To investigate this possibility in detail, we gated Cav1-vesicles into EGF-positive (EGF-colocalizing) or EGF-negative (non-colocalizing) and determined the distance to nucleus center for these two subpopulations (see Section 4 for details on image quantification). We found that the EGF-positive subpopulation of Cav1-vesicles shows a significant shift towards the perinuclear region upon EGF stimulation (Fig. 3A, blue bars). In contrast, the EGF-negative sub-population shows no such tendency (Fig. 3A, red bars).

This indicates that a specific subpopulation of Cav1-vesicles associates with EGF endosomes and traffics towards the perinuclear region.

Since EGF vesicles translocate towards the perinuclear region as well (cf. Figs. 2A and S5, [30]), we reasoned that Cav-1 may preferentially associate with perinuclear (but not peripheral) EGF endosomes. In other words, a spatial gradient of Cav1-association may exist within the EGF endosome population. To test for this hypothesis, we gated EGF endosomes into a perinuclear and a peripheral subpopulation and compared the degree of Cav1-colocalization (Fig. 3B). For this analysis, we selected the timepoint $t = 5$ min of stimulation, because at this timepoint, EGF vesicles are distributed approximately equally between the perinuclear and peripheral region (cf. Fig. 2A, and not shown). As a cutoff value to classify endosomes as perinuclear we used a distance from nucleus center of 9.5 urn, as at early timepoints (<=5 min) most vesicles fell above this values, whereas as late timepoints (>=10 min) most vesicles fell below this value (cf. Fig. S5). Indeed, when comparing the fraction of vesicles co-localizing with Cav1 after 5 min of stimulation, we found that approximately 40% of those EGF endosome classified as perinuclear, but only 20% of those classified as peripheral, co-localized with Cav1. The difference between perinuclear and peripheral was statistically significant ($p = 0.018$), and was qualitatively preserved even if different values were chosen for the distance-to-nucleus cutoff.
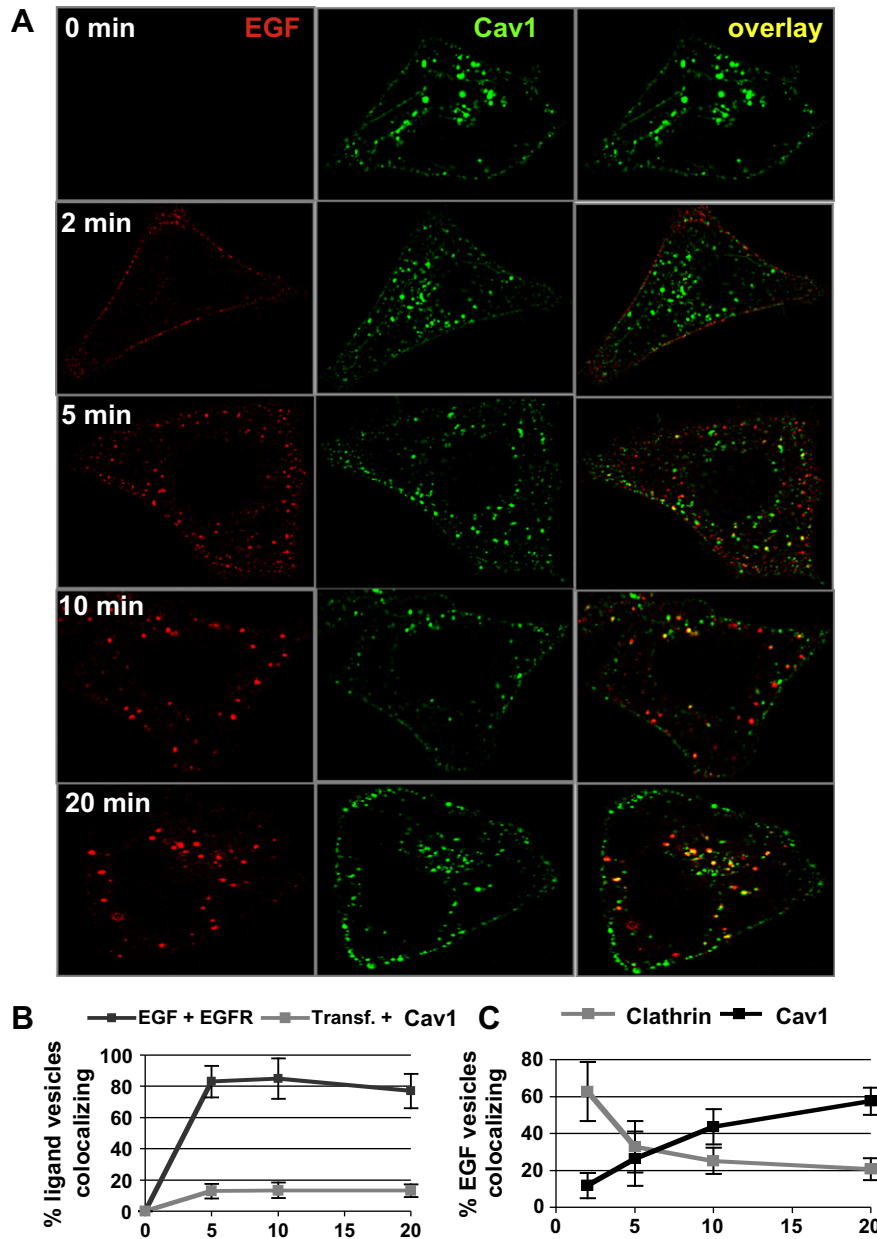
Fig. 2. Specific colocalization between EGF endosomes and Cav1-vesicles increases during endocytic trafficking (A) Confocal microscopy of GFP-Caveolin1 HeLa cells stimulated with Rhodamine-EGF. HeLa cells stably expressing GFP-Cav1 were stimulated with 10 ng/ml with Rhodamine-EGF for the indicated duration, fixed and imaged on a confocal microscope. (B) Control of co-localization analysis. HeLa cells were transfected with GFP-EGFR and stimulated with 10 ng/ml Rhodamine-EGF (dark gray); GFP-Cav1 expressing cells were stimulated with 5 μg/ml Alexa546-Transferrin for the indicated duration (light gray). Prior to imaging, cells were fixed and co-localizing vesicles from both color channels were evaluated from segmented images (see Section 4). In both cases the percentage of ligand vesicles co-localizing with at least one vesicle from the other color channel are shown. Plotted is the mean value of three independent measurements, with 10 cells each. (C) Quantification of co-localization between Rhodamine-EGF and GFP-Cav1 or GFP-clathrin-HC. HeLa cells stably expressing GFP-Cav1 (black) or GFP-clathrin-HC (gray) were stimulated with 10 ng/ml Rhodamine-EGF for the indicated timepoints and co-localization was evaluated as in (B). Plotted is the mean value of three independent measurements, with 10 cells each.

Fig. 3C exemplifies this finding: the pink box marks EGF/Cav1-co-localizing vesicles, which tend to be larger and closer to the nucleus, than non-colocalizing EGF-vesicles, which tend to be small and close to the cell periphery (marked by gray box).

Together, this data shows that a specific subset of Cav1- and EGF-vesicles co-accumulate in growing perinuclear structures.

2.4. Cav1 knockdown perturbs EGF trafficking pattern in late phase of endocytosis

The sustained co-localization that we observed between EGF-endosomes and Cav1-vesicles (cf. Figs. 2 and 3) suggested that

Cav1 regulates endosomal trafficking of EGF. To further test this hypothesis, we examined the effect of Cav1 knockdown on morphology and subcellular distribution of EGF vesicles. Indeed, evaluation of microscopy images revealed that in Cav1-KD cells EGF endosomes showed a markedly different pattern in the late (>10 min) phase of endocytosis, compared to control cells. Fig. 4 shows a time-series of confocal microscopy images of HeLa cells expressing a control vector (upper row) or antisense Cav1 (lower two rows). We provide false-color images of EGF vesicles (upper row-control; middle row – Cav1 KD) to aide the visual comparison of vesicle trafficking patterns. The scale bar on the right indicates pixel intensity – with dark blue being low, and red/orange being
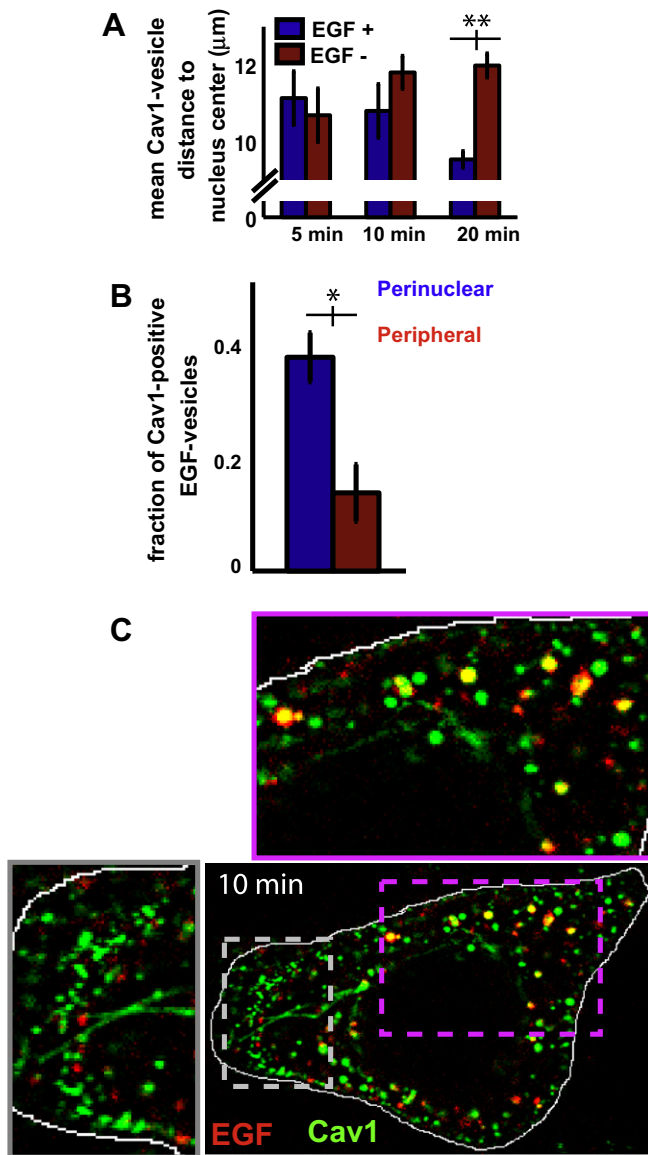
Fig. 3. EGF/Cav1-colocalization shows a spatial gradient towards the perinuclear region (A) HeLa cells stably expressing GFP-Cav1 were stimulated with 10 ng/ml Rhodamine-EGF for the indicated timepoints, fixed and subjected to confocal microscopy. Images were segmented and Cav1-vesicles were gated into EGF-colocalizing (blue) or non-colocalizing (red) and mean Cav1-vesicle distance to nucleus center was determined for both subpopulations. Plotted is the mean value of three measurements, error bars denote standard deviation. 2 stars denote significance of a two-sided t-test at 0.01% level. (B) HeLa cells stably expressing GFP-Cavl were stimulated with 10 ng/ml Rhodamine-EGF for 5 min, fixed and subjected to confocal microscopy. Images were segmented and EGF-vesicles were classified into two subpopulations 'perinuclear' or 'peripheral' depending on their subcellular location (see Section 4 on details how distance to nucleus center was determined for vesicles). An EGF-vesicle was classified as 'perinuclear' if it was located less than 9.5 μm from the center of the nucleus, otherwise as 'peripheral'. For each subpopulation we determined the fraction of vesicles co-localizing with Cavl. Plotted is the mean value of three experiments, error bars denote standard deviation. 1 star denotes significance of a two-sided t-test at 0.1% level. (C) GFP-Cavl expressing HeLa cell stimulated with 10 ng/ml Rhodamine-EGF for 10 min. The cell outline is marked in white.

high intensity. It can be seen that after 5 min of stimulation, the distribution and size of endosomes is similar in control and Cav1-KD cells. However, at later time points, the trafficking pattern in Cav1-KD cells deviates from that in control cells. Whereas in control cells, EGF-vesicles progressively accumulate and cluster in the perinuclear region, vesicles remain dispersed throughout the cytosol in cells lacking Caveolin. This is highlighted in Fig. 4

at timepoints $t = 30$ min, 45 min and 60 min with arrows pointing at EGF vesicles that remain dispersed in the cytosol. We conclude that Cav knockdown alters the spatio-temporal dynamics of late endosomal trafficking of EGF.

2.5. Characterization of EGF endosomal trafficking pattern

To gain more insight into how EGF endosome distribution is affected by Caveolin-depletion, we wished to quantify endosome parameters from microscopy images of cells transfected with a control vector or Cav1-shRNA. To facilitate interpretation, we first conducted a comprehensive analysis of EGF trafficking patterns in unperturbed cells. For this, we extracted the following set of single-endosome or endosome-population parameters from microscopy images at different time points of stimulation: the number of endosomes per cell, endosome distance to nucleus, endosome dispersal (as a measure to reflect the degree of clustering of an endosomes) and endosome EGF content (see Section 4 for details on parameter definition and image analysis). We followed two strategies to describe EGF endosomal trafficking pattern. First, we considered the temporal evolution of mean endosome population values (Fig. S5A–D). We established the following pattern: The mean EGF content per vesicle increased monotonously up to 30 min of stimulation (Fig. S5A). This increase in vesicle cargo content was accompanied by a monotonous decrease of the number of endosomes per cell (Fig. S5B). Together, this suggests that EGF endosomes undergo fusion events, as noted previously [30]. At the same time, EGF vesicles showed a characteristic spatial redistribution: Within 30 min after stimulation, EGF vesicles form clusters in the perinuclear region, visible by a drop in the mean endosome distance to nucleus and in the dispersal of endosomes (Fig. S5C and D).

The temporal evolution of endosome parameters above describes fusion and translocation processes on the endosome population level. However, it is not clear how these events correlate on the level of individual endosomes. To understand the multivariate relationships between parameters on the single-endosome level we applied Bayesian network modeling (see Supporting Text S1 and Fig. S6A). Modeling revealed a robust network of positive and negative parameter dependencies which describes the transition from a population of (i) peripheral vesicles, which are characterized by a small vesicle size, low EGF content, high distance to the nucleus and high degree of dispersal, to (ii) a perinuclear population, characterized by large vesicle size, high EGF content, low distance to the nucleus and low degree of dispersal (see Supporting Text S1 and Fig. S6A and S6B illustrates the pattern of EGF vesicle trafficking as revealed by Bayesian modeling; Fig. S7 shows the histograms of EGF endosome parameters used for modeling). We conclude that in unperturbed conditions, EGF endosomes exhibit a well-defined trafficking pattern.

2.6. Large peripheral EGF endosomes accumulate in Cav1-KD cells

We next analyzed how Cav1 knockdown alters endosomal trafficking of EGF. We first analyzed the temporal evolution of mean endosome parameters. Compared to control cells, the number of EGF vesicles decreased only slightly and not significantly over time in Cav1-depleted cells (Fig. 5A). Thus, in agreement with the flow cytometry results (Fig. 1), the early steps of internalization are unaffected by Caveolin1-depletion: up to 10 min of stimulation, which is when internalization is largely completed, the number of EGF vesicles was comparable between control and Caveolin1-knockdown cells. However, whereas in control cells the number of EGF vesicles had dropped by about 75% after 60 min of stimulation, the number of EGF vesicles in Caveolin1-depleted cells did not change significantly (Fig. 5A).
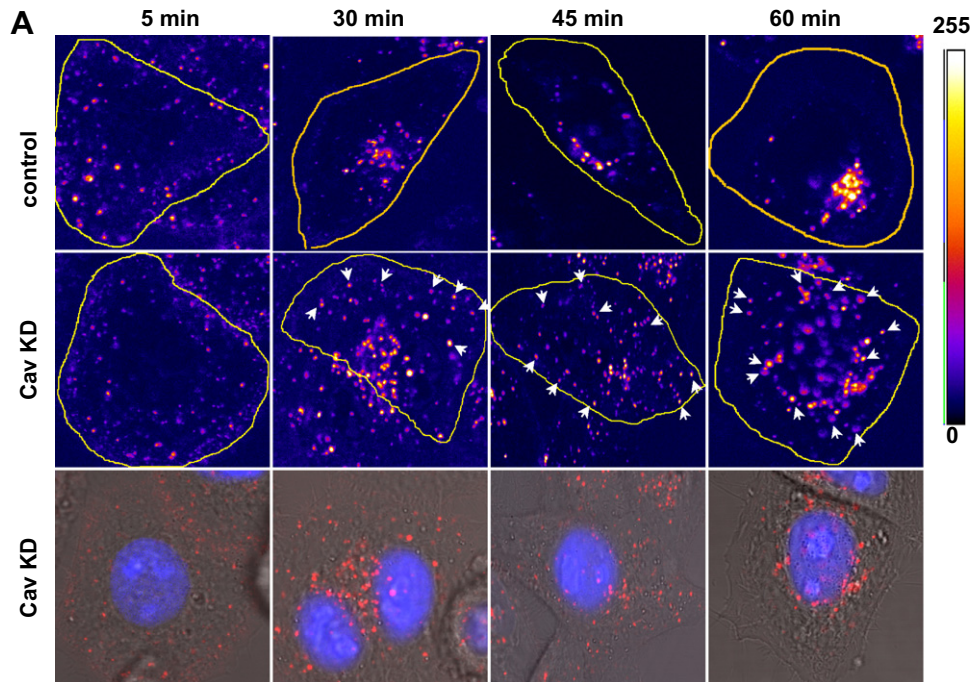
Fig. 4. Effect of Cav1 KD on EGF endocytic trafficking HeLa cells were co-transfected with nuclear-BFP and Cav1 shRNA (lower two rows) or control vector (upper row) in a 1:2 ratio and stimulated with 100 ng/ml Rhodamine-EGF for the indicated duration. To highlight the difference in trafficking patterns in the late phase, we selected three time points from the late phase (30–60 min of stimulation). Further, to facilitate the visual inspection of the images, we show false-color images of control (upper row) and Cav1-KD (middle row) cells. Here, EGF-endosomes are displayed in a color-scheme ranging from dark blue (low intensity) to red/orange/white (high intensity, see color scheme to the right of the figure) and cell outlines are marked in yellow. White arrows mark dispersed vesicles in Cav1-KD cells. The lower row shows the original overlay images of the transmission and fluorescence channels of the Cav1-KD cells in the middle row.
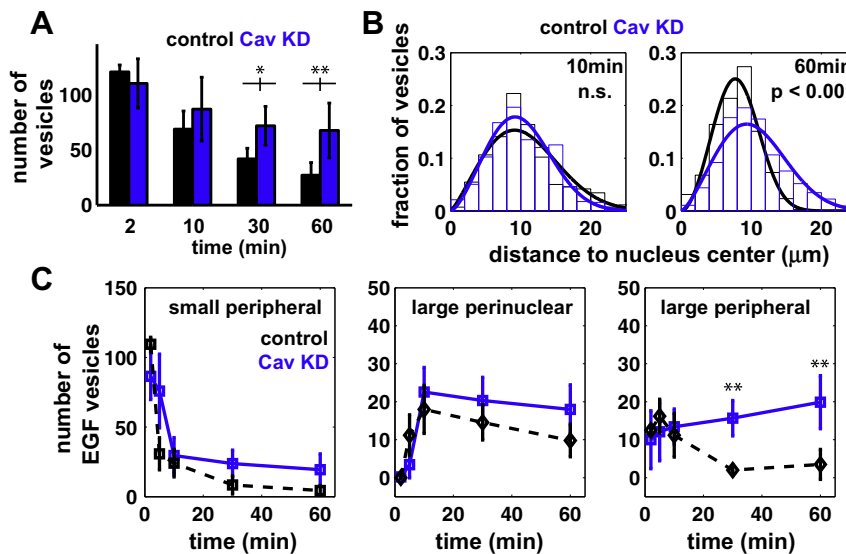
Fig. 5. EGF endocytic trafficking is perturbed in late phase in Cav1 depleted cells. (A) Number of EGF vesicles does not decrease after internalization in Cav1-depleted cells. Quantification of the number of EGF vesicles per cell in one confocal plane in control (black) or Caveolin-depleted (blue) cells. Cells were stimulated with 100 ng/ml Rhodamine-EGF for indicated timepoints, fixed and images were acquired on a confocal microscope. Images were quantified and the number of EGF vesicles per cell was determined. Shown is the mean value of 15 cells, errorbars denote standard deviation between cells from a representative measurement. (B) Trafficking towards perinuclear region is halted in Cav1-depleted cells. Quantification of the distance to nucleus center of EGF vesicles in control (black) or Caveolin-depleted (blue) cells (same data as in A). Shown are histograms and function fits of the distance to nucleus of EGF vesicles after 10 (left) or 60 (right) minutes of stimulation. The number of vesicles for each histogram were: 10 min: 1137 (control) and 1106 (shCav); 60 min: 451 (control) and 901 (shCav). p-value indicates significance level of a paired t-test. (C) Large perinuclear EGF vesicles accumulate in Cav1-depleted but not in control cells. EGF vesicles were gated into four classes according to size and distance to Nucleus center (distToNuc), covering the complete vesicle population: small peripheral (size < 0.45 μm^2, distToNuc >9.5 μm), small perinuclear (size < 0.45 μm^2, distToNuc < 9.5 μm), large perinuclear (size > 0.45 μm^2, distToNuc < 9.5 μm) and large peripheral (size > 0.45 μm^2, distToNuc > 9.5 μm). See Section 4 for selection criteria of threshold values. Shown are the number of vesicles at indicated time points of stimulation for the three classes small peripheral (left), large perinuclear (middle) and large peripheral (right). Two stars denote a p-value <0.01 in a paired test.

We next quantified the subcellular distribution of EGF endosomes in Cav1-depleted and control cells (Fig. 5B). As expected from the visual inspection of the microscopy images (cf. Fig. 4) EGF endosomes fail to accumulate in a perinuclear region in

Caveolin-depleted cells (Fig. 5B). In control cells, the average distance to nucleus center of EGF vesicles decreased from 10.6 μm after 10 min to 7.4 μm after 60 min of stimulation. Moreover, the distribution became narrower, as the coefficient of variation (COV) decreased from 0.41 after 10 min to 0.27 after 60 min of stimulation, indicating that endosomes homogenously accumulated in the perinuclear region in control cells. In Cav1-depleted cells the vesicle distribution was similar to control cells after 10 min (mean = 10.2 μm, COV = 0.42). However, in contrast to control cells the mean distance to nucleus center had not decreased significantly after 60 min (mean = 10.1 μm) in Cav1-KD cells. Furthermore, the distribution had not narrowed, meaning that EGF endosomes remained dispersed throughout the cell (COV = 0.4). This suggests that in Cav1-depleted cells, the progression of endosomes from an early phase, characterized by small size and high distance to the nucleus, to a late stage, characterized by big size and small distance to nucleus, was impaired.

To further investigate, whether a specific subpopulation of EGF vesicles could be identified which was more abundant in Caveolin1 knockdown cells, we gated vesicles into four distinct subpopulations based on their size and subcellular localization. We distinguished the following subpopulations of EGF vesicles: small peripheral, small perinuclear, large peripheral, and large perinuclear (see Section 4 for details on threshold selection). As expected, in control cells EGF vesicles shifted from small peripheral to large perinuclear vesicles within 10 min (Fig. 5C, left and middle panel, black). Similarly, in Caveolin-depleted cells, the population of small peripheral EGF endosomes quickly decreased and large perinuclear endosomes accumulated within 10 min (Fig. 5C, left and middle panel, blue). However, a significant difference emerged in the subclass of large peripheral vesicles, that is, vesicles that have increased in size but have failed to traffic towards the cell interior (Fig. 5C, right panel). Whereas in control cells (black), this class of vesicles practically does not exist, in Caveolin-depleted cells (blue) large peripheral vesicles started to accumulate after 10 min of stimulation. Moreover, the number of vesicles in this class further increased from 30 to 60 min of stimulation. This data demonstrates that Cav1-KD affects the progression of EGF endosomes from small peripheral to large perinuclear endosomes.

We next performed Bayesian modeling on the Cav1-KD endosome data. Bayesian modeling suggested that in Cav1-KD cells, endosome fusion is de-coupled from trafficking towards the nucleus (see Supporting Text S1 and Fig. S6C. S6D illustrates the perturbation of EGF vesicle trafficking as revealed by Bayesian modeling).

In addition, to test how abundance level of Cav1 affects these results, we expressed the Cav1-shRNA vector in the HeLa cell line stably expressing GFP-Cav1 (Fig. S8A and B). This cell line expresses GFP-Cav1 at levels of approximately 50% of the endogeneous protein [24]. We confirmed that even in this environment of Cav1-overexpression, expression of antisense Cav1 resulted in (i) failed perinuclear accumulation (Fig. S8C) and (ii) failed reduction of numbers of EGF vesicles (Figs. S8D and S9).

Together, the presented data demonstrates that Cav1-knockdown perturbs EGF endocytic trafficking and that it leads to the accumulation of large perinuclear endosomes.

2.7. Cav1 KD causes a shift in EGF vesicle distribution towards Rab7-negative compartments at late timepoints

Cav-1 knockdown blocks endosomal progression after 30–45 min of EGF stimulation, a time window where the majority of EGF endosomes is normally found in late endosomal compartments [9,45]. We therefore reasoned that caveolin may control the transition of EGF from an early to a late endosomal compartment.

To analyze the kinetics of late endosome formation in our cells, we co-transfected HeLa cells with a GFP-tagged version of the late endosomal marker Rab7 and imaged cells following stimulation with Alexa555-EGF (Fig. 6A). Since it is possible that Rab7 overexpression affects the flux of EGF endosomes through the endocytic compartments, we attempted to select cells with a low to moderate GFP-Rab7 signal. Substantial co-localization between EGF and Rab7 started to occur after about 10–20 min of stimulation. Thus, EGF-Rab7 colocalization occurs with slower kinetics than EGF-Cav1 colocalization (cf. Fig. 2), supporting that Cav-1 may indeed control the formation of late endosomes.

To confirm acts upstream of Rab7, we analyzed EGF-Rab7 colocalization in HeLa cells harbouring Cav1-shRNA. Similar to control, co-localization between EGF and Rab7 started to occur after about 10–20 min in Cav1 KD cells (Fig. 6B). Evaluation of co-localization revealed that after 45 min of stimulation, EGF vesicles in Cav-1 knockdown cells were equally distributed between Rab7-positive and Rab7-negative structures (Fig. 6D). In contrast, the majority of EGF vesicles was Rab7-positive in control cells, supporting that Cav1-shRNA partly blocks the formation of Rab7-positive endosomes.

Importantly, Rab7 overexpression did not affect the Cav-1 knockdown phenotype, as many dispersed EGF vesicles could be detected in Cav1 knockdown cells (see Fig. 6B and C), while control cells exhibited only few EGF vesicles at 45 min (cf. Fig. 5). Further, we ensured that the analyzed cells showed a similar degree of GFP-Rab7 level between control and Cav1-KD cells.

Taken together, this data shows that Cav1-KD causes an accumulation of EGF endosomes at late timepoints also under Rab7-overexpression conditions. In addition, Cav1-KD causes a shift in EGF vesicle distribution towards Rab7-negative compartments at late timepoints.

3. Discussion

We provided evidence that Caveolin1 is required for proper progression of EGF endosomes but not for EGFR internalization. The presented data suggest a model (cf. Fig. 7) in which EGF:EGFR-complexes are internalized via clathrin-mediated endocytosis into early endosomes and are then sorted into intracellular Cav1-positive vesicles. Expression of a dominant-negative AP180, which is an essential adaptor for clathrin-mediated endocytosis [18], efficiently inhibited EGFR-internalization, and, conversely, EGF-uptake (cf. Fig. 1). In the same line and expectedly, we found that clathrin heavy chain-GFP showed co-localization with small, peripheral EGF-vesicles in a transient manner during the internalization phase (<=10 min after stimulation, cf. Fig. 2C, Fig. S3A and S3B). In contrast, Cav1-vesicles associate only with internalized EGF endosomes after 2–5 min of stimulation.

We used automated image analysis to characterize EGF endosomes and Cav1-vesicles based on a range of parameters such as size and distance to nucleus. The trafficking properties we extracted from images are in accordance with the description of the long-range Caveolae-trafficking mode previously described [31]. First, we found that EGF-positive Cav1-vesicles translocate towards the perinuclear region as EGF endocytic trafficking progresses (cf. Fig. 3A). Moreover, perinuclear EGF endosome co-localize with Cav1 with a higher frequency than peripheral EGF endosomes (cf. Fig. 3B), demonstrating a spatial gradient of co-localization towards the perinuclear region.

Our automated image analysis revealed that Cav1-KD cells drastically affects the EGF trafficking pattern in the late phase of endocytosis (cf. Figs. 4 and 5). Cav1-KD results in (i) failed reduction of endosome numbers (cf. Fig. 5A) and (ii) failed perinuclear accumulation of EGF endosomes (cf. Fig. 5B). Instead, large peripheral
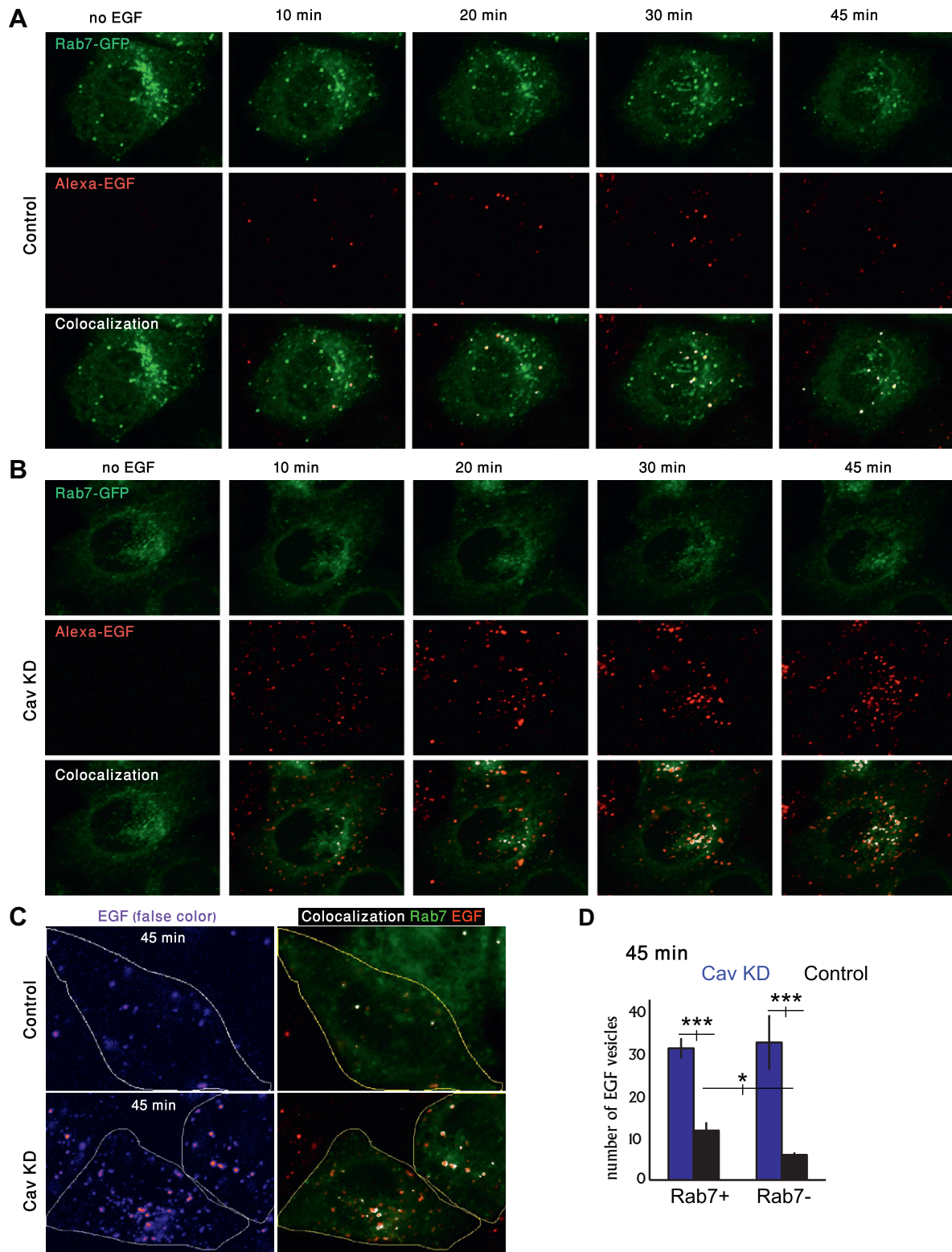
Fig. 6. Cav1-KD causes a shift in EGF vesicle distribution towards Rab7-negative compartments at late timepoints. HeLa cells were co-transfected with GFP-Rab7 and control vector (A) or Cav1-shRNA (B) in a 1:2 ratio, stimulated with 100 ng/ml Alexa-EGF and (live-) imaged on a confocal microscope. Shown are the GFP-Rab7 channel (upper row) or EGF channel (middle row). In the lower row of each panel the overlay images are shown, with co-localization indicated in white. For this visualization of co-localization the ImageJ Plugin 'Colocalization Highlighter' was used. (C) HeLa cells co-transfected with GFP-Rab7 and control (upper) or Cav1-shRNA (lower row) after 45 min of EGF stimulation. The left column shows false-color images of Alexa-EGF, cell outline in white, to facilitate the recognition of differences in number and distribution of EGF vesicles. The second column shows overlay with GFP-Rab7, with colocalization in white. (D) Quantification of EGF/Rab7-colocalization after 45 min of stimulation. Plotted are the number of EGF vesicles that do (left, Rab7+) or do not (right, Rab7−) co-localize with Rab7 in control (black) or Cav1-KD cells (blue). Quantification of co-localization was done using the same code as for Figs. 2 and 3. Shown is the average of 10 cells of a representative experiment, errorbars denote standard deviation between cells.
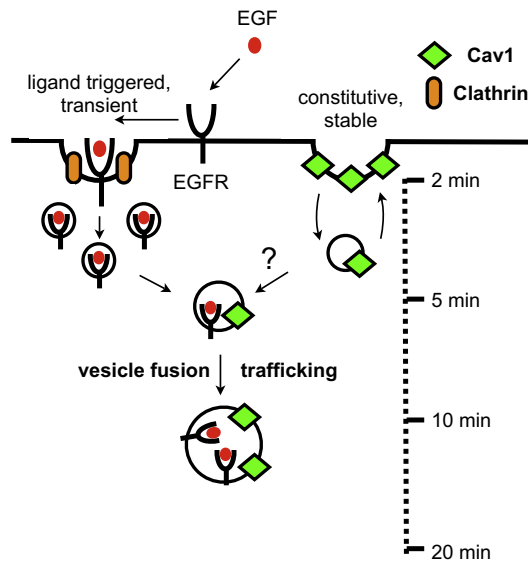
Fig. 7. Model of Caveolae-pathway in EGF endosomal progression EGF stimulation induces internalization of EGF:EGFR complexes via a Clathrin/Ap180-dependent pathway. Internalized Cav1 vesicles interact with early endosomes (marked by low EGF content, proximity to plasma membrane) after 2–5 min of stimulation. The association/fusion (or cargo exchange) between early endosomes and Cav1-vesicles (indicated by a question mark) likely involve local cues not investigated in our study. Clathrin Coated pit assembly is transient, but association of Cav1-vesicles and EGF-containing vesicles is sustained from 5 to 20 min (the time window investigated). Cav1 and EGF-containing vesicles undergo further (i) fusion and (ii) trafficking towards the perinuclear region, whereby the ratio of Cav1/EGF stays approximately constant.

endosomes emerge, which are not observed in control cells (cf. Fig. 5C). Moreover, we found that Cav1 KD affects the distribution of EGF vesicles between endosomal compartments after 45 min of stimulation: whereas in control cells the majority of EGF vesicles colocalizes with the late endosome marker Rab7, in Cav KD cells, EGF vesicles are equally distributed between Rab7-positive and -negative compartments.

Given this evidence, we suggest that Cav1 marks the late endosomal pathway of EGF-trafficking. Support for our conclusion comes from a recent publication, which demonstrated that the intracellular organelles which are marked by the presence of Cav1 and which were originally termed 'caveosome' are in fact identical with late endosomal structures, as judged from co-localization with late endosomal markers Rab7 and Lamp1 [46].

To this date a controversy revolves around the question whether or not a Clathrin-independent Caveolae-internalization pathway exists for EGF:EGFR-complexes. The striking co-localization between EGF/EGFR-endosomes and intracellular Cav1-vesicles has been observed before [13,28]. Based on visual inspection of microscopy images, this prompted the conclusion that EGF:EGFR-complexes internalize via the Caveolae-pathway from the plasma membrane [13,21]. Previous studies addressing the role of Caveolae-mediated trafficking in EGF:EGFR-endocytosis have used nystatin or filipin, which deplete cholesterol from membranes, to disrupt Caveolae-regions [13,14,29]. It was reported that nystatin or filipin treatment reduces uptake of EGF [13,14], which would argue for the existence of internalization pathways that rely on lipid-raft compounds.

However, other studies challenged this observation and reported that nystatin has no effect on EGF-internalization [29]. In contrast to these studies, we specifically addressed the role of Caveolin1, the principal marker of Caveolae-trafficking [22,23,43], by downregulating it using an shRNA. Our automated image analysis approach allowed us a more subtle investigation of (i) the temporal evolution of co-localization, which we found to occur late in

endocytosis and (ii) the type of endosomes that Cav1 co-localized with. This revealed that it is not small, peripheral EGF endosomes which co-localize with Cav1, but rather the large, perinuclear endosomes, reminiscent of late endosomes [9,46]. Thus, in contrast to previous studies we conclude that Cav1 marks only the late phase of EGF endosomal trafficking instead of an independent internalization pathway. Together with the observation that inhibition of Clathrin-mediated endocytosis efficiently inhibits EGF:EGFR internalization as measured in single-cell techniques (cf. Fig. 1A [30]), this suggests that internalized EGF:EGFR-complexes are sorted to the Caveolae-pathway intracellular from endosomes emanating from the Clathrin-pathway (cf. Fig. 6). This trafficking pattern has been observed for certain viral ligands. Cholera Toxin virus and JC virus enter cells via Clathrin mediated internalization and are sorted intracellularly from early endosomes to the caveolar trafficking pathway [31,32], thus showing that the clathrin/endosomal pathway and the Caveolae-trafficking pathway intersect.

Internalization, i.e., translocation of active receptors into the cellular cytosol serves to establish a refractory period in which cells remain insensitive to incoming signal [3]. In addition, experimental evidence suggests that not only internalization, but the subsequent endocytic trafficking of activated EGFR constitutes major regulatory steps in signal regulation (reviewed in [1,47]). This signal-modulating role of endocytic proteins may stem from its function in placing the active receptors in contact with intracellular signaling complexes [48].

Receptors remain active in endosomes and proper trafficking is often required for sustained signaling [14]. Consequently it is likely that a delay in the progression through the correct endosomal compartment will corrupt and potentially enhance normal signaling. Caveolin1 is known to attenuate growth factor signaling, but the mechanistic basis as to how it acts on growth factor signaling has not been investigated. Cellular regulation of caveolin expression levels strongly correlates with growth inhibition [35,49]. Cells grown to confluency as well cells deprived of growth factors upregulate caveolin expression, with lowest caveolin levels found during exponential growth phase [35]. Importantly, Cav1 expression has been found to be greatly reduced in many human cancer cells [7] and a mutant form of Cav1 has been identified in 16% of primary human breast cancers [50]. Loss of stromal caveolin-1 expression predicts poor clinical outcome in certain types of breast cancers [51]. We propose that the failure of EGF endosomes to progress to the perinuclear region, the increased total number of EGF endosomes and the changed morphology of EGF endosomes form a mechanistic basis for the observations that Cav1-deletion or mutations results in enhanced growth factor signaling.

4. Material and methods

4.1. Cell culture and treatment

HeLa cells were grown at 37 °C in Dulbecco's modified Eagle's medium containing 10% fetal bovine serum (FBS) and 1% penicillin and streptomycin (P/S) and were maintained in a humidified incubator with 5% CO_2. To synchronize the cells before stimulation with EGF, cells were serum starved over night when they reached 80% confluence. EGF was added to a final concentration indicated for different times at 37 °C in a humidified and 5% CO_2 atmosphere. After treatment the cells were washed twice with ice-cold phosphate-buffered saline (PBS) and further analyses were performed.

4.2. Detection of EGF:EGFR internalization (flow cytometry)

Internalization of Rhodamine-EGF was detected using flow cytometry as described previously [7]. Briefly, to measure EGF-up-

take, cells were stimulated with Rhodamine-EGF directly in the starvation medium at the indicated concentration, followed by wash with acid stripping buffer (50 mM glycine, 150 mM NaCl, pH 3.0), then washed with PBS, followed by trypsination and resuspension in full medium prior to flow cytometric analysis.

To detect surface-EGFR using flow cytometry, cells were treated and stimulated with EGF as described above.

After removal of EGF by washing with ice-cold PBS, the cells were trypsinized and fixed in 3% paraformaldehyde for 15 min. After washing twice with PBS, the cells were incubated with 50 mM ammoniumchlorid/PBS for 10 min to saturate free aldehyde-groups followed by a next washing step. Cells were blocked with 0.03% BSA/PBS for 30 min at room temperature and incubated with mouse anti-EGFR (1:50) for 1 h at room temperature. The cells were washed again and goat anti-mouse IgG conjugated with Alexa 594 (1:600) for 1 h at room temperature. Samples were measured on a modified flow cytometer: FC500/MPL (Beckman Coulter).

4.3. Microscopy

Cells were imaged on a confocal laser scanning microscope TCS SP5 (Leica Microsystems, Wetzlar, Germany) using a 63x oil immersion objective.

A helium/neon ($A = 543$ nm) laser was used for excitation of Rhodamine or Alexa555, an argon laser ($A = 488$ nm) for excitation of GFP and a UV-laser ($A = 405$ nm) for excitation of BFP. For fixation, cells were washed in PBS once, fixed in 4% PFA for 10 min on ice and then returned to PBS for imaging.

4.4. Antibodies and chemicals

Mouse anti-EGFR (1005) antibody was from Santa Cruz. Secondary antibody for indirect immunofluorescence was goat anti-mouse Alexa 488 from molecular probes. Tetramethylrhodamine-EGF (Rh-EGF), Alexa-555-EGF and Alexa-555-Transferrin were from Invitrogen, Carlsbad.

4.5. Cell transfection and plasmids

Cells were transfected using lipofectamine transfection agent following the standard protocol. To generate AP180mut-IRES-GFP, we cloned the cDNA coding for the truncated form of AP180 [18] in the multiple cloning site of the pIRES-Neo3 vector (Clontech) and replaced the neomycin phosphotransferase coding sequence of the vector with the one of EGFP. For co-transfection assays, plasmid DNA was mixed in a 1:2 ratio and then the standard transfection protocol was used. The construct of truncated AP180 was a kind gift from Harvey McMahon [18]. Caveolin1-shRNA was a kind gift from Walter Atwood [32].

4.6. Image processing

4.6.1. Image segmentation and vesicle detection

Microscopy images were segmented using a watershed algorithm, involving the following steps: first, background noise was subtracted using a rolling ball median filter with a radius of 7 pixels. Next, a watershed-segmentation was performed [52] and vesicles were detected according to the parameters: X/Y-coordinate of center of mass, size and integrated pixel intensity. For segmentation and vesicle detection, existing methods from the open-source software ImageJ [52] were used and arranged in a custom-made macro (available upon request).

4.6.2. Definition of vesicle parameters

From an endosome's X/Y-coordinates (see above), the endosomes's (i) distance to nucleus center and (ii) dispersal were

calculated. An endosome's distance to nucleus center was calculated as follows: For each cell analyzed, a transmission image was recorded in addition to the fluorescence channel. From this transmission image, the center of nucleus was taken and for each endosome of this cell, the distance to nucleus center was calculated as the euclidean distance. Endosome dispersal was defined as the median value of all $(n-1)$-pairwise distances of an endosome to all other endosomes from the same cell. For these calculations, MATLAB scripts were written.

4.6.3. Detection of co-localization

Co-localization between vesicles from different color channels was calculated from the segmented images. Two vesicles were judged as co-localized, if their respective centers of mass were localized less than 0.3 μm apart. Co-localization analysis was done in MATLAB.

4.6.4. Gating of vesicles

EGF endosomes were gated into four distant subpopulations based on size and distance to nucleus (D). Endosomes were categorized as 'small' when their area was less than 0.45 μm^2, which has been found as the typical size of late endosomes [53]. Endosomes were classified as peripheral, when their distance to nucleus center (D) was larger than 9.5 μm, which we found a good discriminator to distinguish between the early endosome population and the late, perinuclear population. Specifically, endosomes were classified: Small peripheral: size < 0.45 μm^2 and D > 9.5 μm. Large peripheral: size >0.45 μm^2 and D > 9.5 μm. Large perinuclear: size > 0.45 μm^2 and D < 9.5 μm. Small perinuclear: size < 0.45 μm^2 and D < 9.5 μm.

4.6.5. Bayesian modeling of endosome parameters

Inducing a Bayesian network model from data consists of two procedures: (a) learning a network structure by searching in space of possible graphical models consistent with conditional independencies suggested by the data and (b) inferring the parameters of the conditional probabilities encoded in the network structure found. The first procedure uses a scoring function that evaluates each candidate model by its posterior probability given the data (Bayesian approach). We learned 2 Bayesian networks for control and Caveolin1 knockdown cells at 10 min of EGF stimulation from the data on endosome parameters size, EGF content, distance to nucleus.

Dispersal, number of endosomes per cell. Parameters were discretized into two values "low" and "high". Discretization thresholds were determined based on histograms of distributions of the endosome parameters (Fig. S7), as well as on the literature values. Further thresholds were: EGF content: 8000 (pixel intensity), Distance to nucleus center: 9.5 μm, Dispersal: 9 μm, number of endosomes: 55. For network learning we used the R package deal (http://cran.r-project.org/) and our own implementation, which is available upon request. As search strategy a greedy search with random restarts was used. To increase the degree of confidence in the network learning, we generated 100 Bayesian Networks and selected the best scoring network.

Appendix A. Supplementary data

Supplementary data associated with this article can be found, in the online version, at doi:10.1016/j.febslet.2012.02.041.

References

[1] Scita, G. and Di Fiore, P.P. (2010) The endocytic matrix. Nature 463, 464–473.
[2] Mosesson, Y., Mills, G.B. and Yarden, Y. (2008) Derailed endocytosis: an emerging feature of cancer. Nat. Rev. Cancer 8, 835–850.

[3] Wiley, H.S. and Burke, P.M. (2001) Regulation of receptor tyrosine kinase signaling by endocytic trafficking. Traffic 2, 1218.

[4] Marmor, M.D., Skaria, K.B. and Yarden, Y. (2004) Signal transduction and oncogenesis by ErbB/HER receptors. Int. J. Radiat. Oncol. Biol. Phys. 58, 903–913.

[5] Citri, A. and Yarden, Y. (2006) EGF-ERBB signalling: towards the systems level. Nat. Rev. Mol. Cell Biol. 7, 505–516.

[6] Wiley, H.S. (2003) Trafficking of the ErbB receptors and its influence on signaling. Exp. Cell Res. 284, 78–88.

[7] Schmidt-Glenewinkel, H., Reinz, E., Eils, R. and Brady, N.R. (2009) Systems biological analysis of epidermal growth factor receptor internalization dynamics for altered receptor levels. J. Biol. Chem. 284, 17243–17252.

[8] Mellman, I. (1996) Endocytosis and molecular sorting. Annu. Rev. Cell Dev. Biol. 12, 575–625.

[9] Rink, J., Ghigo, E., Kalaidzidis, Y. and Zerial, M. (2005) Rab conversion as a mechanism of progression from early to late endosomes. Cell 122, 735–749.

[10] Vieira, A.V., Lamaze, C. and Schmid, S.L. (1996) Control of EGF receptor signaling by clathrin-mediated endocytosis. Science 274, 2086–2089.

[11] Miaczynska, M., Pelkmans, L. and Zerial, M. (2004) Not just a sink: endosomes in control of signal transduction. Curr. Opin. Cell Biol. 16, 400–406.

[12] Lenferink, A.E., Pinkas-Kramarski, R., Poll, M.L.V.D., Vugt, M.J.V., Klapper, L.N., et al. (1998) Differential endocytic routing of homo- and hetero-dimeric ErbB tyrosine kinases confers signaling superiority to receptor heterodimers. EMBO J. 17, 3385–3397.

[13] Sigismund, S., Woelk, T., Puri, C., Maspero, E., Tacchetti, C., et al. (2005) Clathrin-independent endocytosis of ubiquitinated cargos. Proc. Natl. Acad. Sci. USA 102, 2760–2765.

[14] Sigismund, S., Argenzio, E., Tosoni, D., Cavallaro, E., Polo, S., et al. (2008) Clathrin-mediated internalization is essential for sustained EGFR signaling but dispensable for degradation. Dev. Cell 15, 209–219.

[15] Mettlen, M., Loerke, D., Yarar, D., Danuser, G. and Schmid, S.L. (2010) Cargo- and adaptor-specific mechanisms regulate clathrin-mediated endocytosis. J. Cell Biol. 188, 919–933.

[16] Sorkin, A. and Goh, L.K. (2009) Endocytosis and intracellular trafficking of ErbBs. Exp. Cell Res. 315, 683–696.

[17] Sorkin, A. (2004) Cargo recognition during clathrin-mediated endocytosis: a team effort. Curr. Opin. Cell Biol. 16, 392–399.

[18] Ford, M.G., Pearse, B.M., Higgins, M.K., Vallis, Y., Owen, D.J., et al. (2001) Simultaneous binding of PtdIns(4,5)P2 and clathrin by AP180 in the nucleation of clathrin lattices on membranes. Science 291, 1051–1055.

[19] Mettlen, M., Loerke, D., Yarar, D., Danuser, G. and Schmid, S.L. (2010) Cargo- and adaptor-specific mechanisms regulate clathrin-mediated endocytosis. J. Cell Biol. 188, 919–933.

[20] Mettlen, M., Pucadyil, T., Ramachandran, R. and Schmid, S.L. (2009) Dissecting dynamin's role in clathrin-mediated endocytosis. Biochem. Soc. Trans. 37, 1022–1026.

[21] Aguilar, R.C. and Wendland, B. (2005) Endocytosis of membrane receptors: two pathways are better than one. Proc. Natl. Acad. Sci. USA 102, 2679–2680.

[22] Mundy, D.I., Machleidt, T., Ying, Y., Anderson, R.G.W. and Bloom, G.S. (2002) Dual control of caveolar membrane traffic by microtubules and the actin cytoskeleton. J. Cell Sci. 115, 4327–4339.

[23] Pelkmans, L. and Helenius, A. (2002) Endocytosis via caveolae. Traffic 3, 311–320.

[24] Pelkmans, L. and Zerial, M. (2005) Kinase-regulated quantal assemblies and kiss-and-run recycling of caveolae. Nature 436, 128–133.

[25] Pelkmans, L., Burli, T., Zerial, M. and Helenius, A. (2004) Caveolin-stabilized membrane domains as multifunctional transport and sorting devices in endocytic membrane traffic. Cell 118, 767–780.

[26] Huang, F., Khvorova, A., Marshall, W. and Sorkin, A. (2004) Analysis of clathrin-mediated endocytosis of epidermal growth factor receptor by RNA interference. J. Biol. Chem. 279, 16657–16661.

[27] Hinrichsen, L., Harborth, J., Andrees, L., Weber, K. and Ungewickell, E.J. (2003) Effect of clathrin heavy chain- and alpha-adaptin-specific small inhibitory RNAs on endocytic accessory proteins and receptor trafficking in HeLa cells. J. Biol. Chem. 278, 45160–45170.

[28] Khan, E.M., Heidinger, J.M., Levy, M., Lisanti, M.P., Ravid, T., et al. (2006) Epidermal growth factor receptor exposed to oxidative stress undergoes Src- and caveolin-1-dependent perinuclear trafficking. J. Biol. Chem. 281, 14486–14493.

[29] Kazazic, M., Roepstorff, K., Johannessen, L.E., Pedersen, N.M., Deurs, B.V., et al. (2006) EGF-induced activation of the EGF receptor does not trigger mobilization of caveolae. Traffic 7, 1518–1527.

[30] Collinet, C., Stoter, M., Bradshaw, C.R., Samusik, N., Rink, J.C., et al. (2010) Systems survey of endocytosis by multiparametric image analysis. Nature 464, 243–249.

[31] Pelkmans, L., Burli, T., Zerial, M. and Helenius, A. (2004) Caveolin-stabilized membrane domains as multifunctional transport and sorting devices in endocytic membrane traffic. Cell 118, 767–780.

[32] Querbes, W., O'Hara, B.A., Williams, G. and Atwood, W.J. (2006) Invasion of host cells by JC virus identifies a novel role for caveolae in endosomal sorting of noncaveolar ligands. J. Virol. 80, 9402–9413.

[33] Williams, T.M. and Lisanti, M.P. (2005) Caveolin-1 in oncogenic transformation, cancer, and metastasis. Am. J. Physiol. Cell Physiol. 288, C494–C506.

[34] Lisanti, M.P., Tang, Z., Scherer, P.E., Kubler, E., Koleske, A.J., et al. (1995) Caveolae, transmembrane signalling and cellular transformation. Mol. Membr. Biol. 12, 121–124.

[35] Galbiati, F., Volonte, D., Engelman, J.A., Watanabe, G., Burk, R., et al. (1998) Targeted downregulation of caveolin-1 is sufficient to drive cell transformation and hyperactivate the p42/44 MAP kinase cascade. EMBO J. 17, 6633–6648.

[36] Engelman, J.A., Wykoff, C.C., Yasuhara, S., Song, K.S., Okamoto, T., et al. (1997) Recombinant expression of caveolin-1 in oncogenically transformed cells abrogates anchorage-independent growth. J. Biol. Chem. 272, 16374–16381.

[37] Fiucci, G., Ravid, D., Reich, R. and Liscovitch, M. (2002) Caveolin-1 inhibits anchorage-independent growth, anoikis and invasiveness in MCF-7 human breast cancer cells. Oncogene 21, 2365–2375.

[38] Han, F., Gu, D., Chen, Q. and Zhu, H. (2009) Caveolin-1 acts as a tumor suppressor by down-regulating epidermal growth factor receptor-mitogen-activated protein kinase signaling pathway in pancreatic carcinoma cell lines. Pancreas 38, 766–774.

[39] Benmerah, A., Bayrou, M., Cerf-Bensussan, N. and Dautry-Varsat, A. (1999) Inhibition of clathrin-coated pit assembly by an Eps15 mutant. J. Cell Sci. 112 (Pt 9), 1303–1311.

[40] Hoffmann, A., Dannhauser, P.N., Groos, S., Hinrichsen, L., Curth, U., et al. (2010) A comparison of GFP-tagged clathrin light chains with fluorochromated light chains in vivo and in vitro. Traffic 11, 1129–1140.

[41] Kirchhausen, T., Boll, W., Oijen, A.V. and Ehrlich, M. (2005) Single-molecule live-cell imaging of clathrin-based endocytosis. Biochem. Soc. Symp., 71–76.

[42] Haglund, K., Sigismund, S., Polo, S., Szymkiewicz, I., Fiore, P.P.D., et al. (2003) Multiple monoubiquitination of RTKs is sufficient for their endocytosis and degradation. Nat. Cell Biol. 5, 461–466.

[43] Tagawa, A., Mezzacasa, A., Hayer, A., Longatti, A., Pelkmans, L., et al. (2005) Assembly and trafficking of caveolar domains in the cell: caveolae as stable, cargo-triggered, vesicular transporters. J. Cell Biol. 170, 769–779.

[44] Pelkmans, L., Burli, T., Zerial, M. and Helenius, A. (2004) Caveolin-stabilized membrane domains as multifunctional transport and sorting devices in endocytic membrane traffic. Cell 118, 767–780.

[45] Waterman, H. and Yarden, Y. (2001) Molecular mechanisms underlying endocytosis and sorting of ErbB receptor tyrosine kinases. FEBS Lett. 490, 142–152.

[46] Hayer, A., Stoeber, M., Ritz, D., Engel, S., Meyer, H.H., et al. (2010) Caveolin-1 is ubiquitinated and targeted to intralumenal vesicles in endolysosomes for degradation. J. Cell Biol. 191, 615–629.

[47] Mosesson, Y., Mills, G.B. and Yarden, Y. (2008) Derailed endocytosis: an emerging feature of cancer. Nat. Rev. Cancer 8, 835–850.

[48] Hoeller, D., Volarevic, S. and Dikic, I. (2005) Compartmentalization of growth factor receptor signalling. Curr. Opin. Cell Biol. 17, 107–111.

[49] Koleske, A.J., Baltimore, D. and Lisanti, M.P. (1995) Reduction of caveolin and caveolae in oncogenically transformed cells. Proc. Natl. Acad. Sci. USA 92, 1381–1385.

[50] Hayashi, K., Matsuda, S., Machida, K., Yamamoto, T., Fukuda, Y., et al. (2001) Invasion activating caveolin-1 mutation in human scirrhous breast cancers. Cancer Res. 61, 2361–2364.

[51] A.K. Witkiewicz, A. Dasgupta, S. Sammons, O. Er, M.B. Potoczek et al., Loss of stromal caveolin-1 expression predicts poor clinical outcome in triple negative and basal-like breast cancers. Cancer Biol. Ther. 10, Available at: <http://www.ncbi.nlm.nih.gov/pubmed/20431349>, 2010 (accessed 14.10.2010).

[52] Abramoff, M., Magelhaes, P. and Ram, S. (2004) Image processing with image. J. Biophoton. Int. 11, 36–42.

[53] Ganley, I.G., Carroll, K., Bittova, L. and Pfeffer, S. (2004) Rab9 GTPase regulates late endosome size and requires effector interaction for its stability. Mol. Biol. Cell 15, 5420–5430.